Molecular Biology of the Cell
Vol. 19, 5506–5516, December 2008

Self-Interaction Is Critical for Atg9 Transport and Function at the Phagophore Assembly Site during Autophagy

Congcong He,* Misuzu Baba,† Yang Cao,* and Daniel J. Klionsky*

*Life Sciences Institute and Departments of Molecular, Cellular and Developmental Biology, and Biological Chemistry, University of Michigan, Ann Arbor, MI 48109; and †Department of Chemical and Biological Sciences, Faculty of Science, Japan Women's University, Mejirodai, Tokyo 112-8681, Japan

Submitted May 30, 2008; Revised September 22, 2008; Accepted September 23, 2008
Monitoring Editor: Jeffrey L. Brodsky

Autophagy is the degradation of a cell's own components within lysosomes (or the analogous yeast vacuole), and its malfunction contributes to a variety of human diseases. Atg9 is the sole integral membrane protein required in formation of the initial sequestering compartment, the phagophore, and is proposed to play a key role in membrane transport; the phagophore presumably expands by vesicular addition to form a complete autophagosome. It is not clear through what mechanism Atg9 functions at the phagophore assembly site (PAS). Here we report that Atg9 molecules self-associate independently of other known autophagy proteins in both nutrient-rich and starvation conditions. Mutational analyses reveal that self-interaction is critical for anterograde transport of Atg9 to the PAS. The ability of Atg9 to self-interact is required for both selective and nonselective autophagy at the step of phagophore expansion at the PAS. Our results support a model in which Atg9 multimerization facilitates membrane flow to the PAS for phagophore formation.

INTRODUCTION

Autophagic degradation of unneeded or damaged cellular components is essential for various cellular functions including proper homeostasis. Along these lines, the malfunction of autophagy is implicated in a variety of diseases, including cancer, neurodegeneration, cardiac disorders, and pathogen infection (Shintani and Klionsky, 2004a). During autophagy, cytosolic proteins and organelles are engulfed into a double-membrane vesicle, the autophagosome, which then fuses with a lysosome (or the vacuole in fungi and plants) where its cargos are degraded. The autophagy-related (Atg) protein Atg9 plays a central role in the nucleation step during autophagosome formation in eukaryotes ranging from yeast to mammals (Noda *et al.*, 2000; Young *et al.*, 2006). Being the only identified integral membrane protein that is absolutely required in autophagosome formation, Atg9 is proposed to be the "carrier" of lipids to the phagophore assembly site (PAS, also known as the preautophagosomal structure; Kim *et al.*, 2002). Atg9 is absent from the completed autophagosomes, suggesting that the protein is retrieved upon vesicle completion. Previous work done in the yeast *Saccharomyces cerevisiae* has shown that Atg9 interacts with multiple autophagy-related proteins via its two cytosol-facing termini (Reggiori *et al.*, 2005; He *et al.*, 2006; Legakis *et al.*, 2007; Yen *et al.*, 2007). However, the physiological role of such a multisubunit complex in autophagy and the function of Atg9 in this complex are still unclear.

Selective autophagy, such as pexophagy (degradation of excess peroxisomes), mitophagy (clearance of damaged mitochondria), and the cytoplasm-to-vacuole targeting (Cvt) pathway, targets specific cargos (Xie and Klionsky, 2007). The Cvt pathway occurs during vegetative growth in yeast, in which two vacuolar hydrolases, α-mannosidase and the precursor form of aminopeptidase I (Ape1 [prApe1]), are transported to the vacuole where prApe1 is processed into mature Ape1. Nonselective, bulk autophagy occurs at a basal level and is induced by developmental signals and/or stress conditions (Levine and Klionsky, 2004). For instance, during starvation, nutrients are provided to ensure cell survival through elevated autophagic degradation of bulk cytoplasm and subsequent release of the breakdown products from the lysosome. Previous studies in yeast show a cycling route of Atg9 transport between the PAS and some peripheral compartments including mitochondria, during vegetative growth: the anterograde transport of Atg9 to the PAS facilitated by Atg9 binding partners may deliver lipids to the PAS, and the retrieval of Atg9 from the PAS may recycle the protein back to the membrane origin for the next round of delivery (Reggiori *et al.*, 2004a; He *et al.*, 2006). Nevertheless, to date little is known about the mechanism targeting Atg9 to the PAS during starvation-induced bulk autophagy.

Unlike other intracellular trafficking vesicles that usually bud from the surface of a preexisting organelle, an autophagosome is thought to assemble by fusion of new membrane fragments with the phagophore, the initial sequestering compartment, at the PAS. However, the membranous structure at the PAS, or the expanding phagophore, has not been clearly elucidated; how small membranes are incorporated into this structure remains unknown. In this article, we present data that Atg9 interacts with itself in both nutrient-rich and starvation conditions independent of other Atg proteins. The self-interaction, which is mediated by the C

This article was published online ahead of print in *MBC in Press* (http://www.molbiolcell.org/cgi/doi/10.1091/mbc.E08–05–0544) on October 1, 2008.

Address correspondence to: Daniel J. Klionsky (klionsky@umich.edu).

Abbreviations used: Ape1, aminopeptidase I; Atg, autophagy-related; Cvt, cytoplasm to vacuole targeting; MKO, multiple-knockout; PAS, phagophore assembly site; prApe1, precursor aminopeptidase I; SNARE, *N*-ethylmaleimide-sensitive factor attachment protein receptor.

Table 1.

Yeast strains used in this study

Strain	Genotype	Reference
BY4742	*MATα ura3Δ leu2Δ his3Δ lys2Δ*	Invitrogen
CCH001	SEY6210 *atg9Δ::HIS5 atg1Δ::LEU2*	He *et al.* (2006)
CCH002	YTS158 *atg9Δ::HIS5*	He *et al.* (2006)
CCH010	YCY123 *ATG9–3GFP::URA3 ATG9-3DsRed::LEU2*	This study
CCH011	SEY6210 *ATG9–3GFP::URA3 ATG9–3DsRed::LEU2*	This study
CCH019	SEY6210 *ATG9-TAP::TRP1*	This study
CCH020	JLY68 *atg9Δ::LEU2*	This study
CCH025	SEY6210 *RFP-APE1::LEU2 atg9Δ::HIS3*	This study
CCH026	SEY6210 *ATG14-GFP::TRP1 RFP-APE1::LEU2 atg9Δ::HIS3*	This study
CCH027	SEY6210 *atg9Δ::TAP(URA3)*	This study
JKY007	SEY6210 *atg9Δ::HIS3*	Noda *et al.* (2000)
JLY68	SEY6210 *ATG23-PA::HIS5 ATG27-HA::TRP1*	Legakis *et al.* (2007)
PJ69–4A	*MATα leu2–3,112 trp1-Δ901 ura3–52 his3-Δ200 gal4Δ gal80Δ LYS2::GAL1-HIS3 GAL2-ADE2 met2::GAL7-lacZ*	James *et al.* (1996)
SEY6210	*MATα ura3–52 leu2–3,112 his3-Δ200 trp1-Δ901 lys2–801 suc2-Δ9 mel GAL*	Robinson *et al.* (1988)
UNY102	SEY6210 *TAP-ATG1*	Yorimitsu *et al.* (2006)
YCY123	SEY6210 *atg1Δ, 2Δ, 3Δ, 4Δ, 5Δ, 6Δ, 7Δ, 8Δ, 9Δ, 10Δ, 11Δ, 12Δ, 13Δ, 14Δ, 16Δ, 17Δ, 18Δ, 19Δ, 20Δ, 21Δ, 23Δ, 24Δ, 27Δ, 29Δ*	Cao *et al.* (2008)
YCY135	YCY123 *ATG9–3GFP::URA3*	This study
YTS158	BY4742 *pho8::pho8Δ60 pho13Δ::KAN*	He *et al.* (2006)

terminus of the protein, promotes the trafficking of Atg9 from its origins to the PAS and is required for both selective and nonselective starvation-induced autophagy. Through examining the expansion of Atg9-containing phagophores by fluorescence and immunoelectron microscopy, we found that the ability of Atg9 to multimerize is an essential function during formation of a normal phagophore at the PAS. Our data provide new conceptual insights to the molecular mechanism governing Atg9 anterograde transport and assembly of the PAS during bulk autophagy and hence refine the cycling model of Atg9 transport.

MATERIALS AND METHODS

Yeast Strains and Media

The *S. cerevisiae* strains used in this study are listed in Table 1. For disruption of *ATG9*, the entire coding region was replaced by the *Kluyveromyces lactis LEU2* gene using PCR primers containing ~45 bases of identity to the regions flanking the open reading frame. For PCR-based integration of the green fluorescent protein (GFP) or tandem affinity purification (TAP) tag, pFA6a-GFP(S65T)-TRP1, or pBS1479 and pBS1539, was used as the template, respectively (Longtine *et al.*, 1998; Puig *et al.*, 2001). For integration of the Atg9-3GFP fusion, the integrative plasmid pATG9–3GFP(306) was linearized by digestion with StuI and integrated into the *URA3* gene locus. For integration of the Atg9-3DsRed fusion, the DNA fragment containing the *ATG9* gene and native promoter was released from pATG9–3GFP(306) and cloned into pTPIARP2–3DsRed(305) using XhoI and BamHI; the resulting integrative plasmid pAtg9-3DsRed(305) was linearized by digestion with AflII and integrated into the *LEU2* gene locus.

Yeast cells were grown in rich medium (YPD; 1% yeast extract, 2% peptone, 2% glucose) or synthetic minimal medium (SMD; 0.67% yeast nitrogen base, 2% glucose, amino acids, and vitamins as needed). Starvation experiments were conducted in synthetic medium lacking nitrogen (SD-N; 0.17% yeast nitrogen base without amino acids and 2% glucose).

Plasmids

Plasmids expressing HA-Atg13 (pHAAtg13(315); Cheong *et al.*, 2008), RFP-Ape1 (pRFPApe1(414); Stromhaug *et al.*, 2004), GFP-Atg8 (pGFP-AUT7(414); Abeliovich *et al.*, 2003); Atg9 (pAPG9(416), essentially constructed the same as pAPG9(414); Noda *et al.*, 2000); Atg9-GFP (pAPG9GFP(416) and pCuAPG9GFP(416); Noda *et al.*, 2000); Atg9-PA (pAtg9PA(314); He *et al.*, 2006); HA-Atg11 (pCuHA-CVT9(414); Kim *et al.*, 2001); cyan fluorescent protein (CFP)-Atg11 (pCuHACFPCVT9(414); Kim *et al.*, 2002); GFP-Atg2 (pCuGFPAPG2(414); Wang *et al.*, 2001); and Atg18-GFP (pCVT18GFP(414); Guan *et al.*, 2001) have been described previously. Yeast two-hybrid plasmids expressing Atg11 (pAD-Atg11), Atg18 (pAD-Atg18), Atg23 (pAD-Atg23), Atg27 (pAD-Atg27), Atg9 (pAD-Atg9 and pBD-Atg9), and the Atg9 N terminus (pAD-Atg9N) or the C terminus (pAD-Atg9C) have been described previously (He *et al.*, 2006).

The plasmids pAtg9Δ787-997(416) and pAtg9Δ870-997(416) were generated by amplifying the Atg9Δ787-997 and Atg9Δ870-997 fragments from pAPG9(416) and cloning them into the two AatII sites in pAPG9(416). To generate the plasmid expressing Atg9Δ766-997-GFP driven by the *TPI1* promoter (pS1S2(416)), the N terminus of *ATG9* (928 base pairs) was amplified and cloned in the vector pPEP416 (Reggiori *et al.*, 2000) digested with EcoRI/SacII. The 3′ primer introduced an XbaI site and a SacII site preceded by a stop codon. The resulting pS1(416) plasmid was then cut with XbaI/SacII, and the central part of *ATG9* (1404 base pairs) was amplified and inserted using the same enzymes. For internal deletions of Atg9 (Atg9Δ766-785-GFP, Atg9Δ766-770-GFP, Atg9Δ771-775-GFP, Atg9Δ776-780-GFP and Atg9Δ781-785-GFP), the truncated open reading frames were amplified by PCR and cloned into NotI and BamHI sites of pAPG9GFP(416). For generation of nontagged pAtg9Δ766-785(416), pAtg9Δ766-770(416), pAtg9Δ781-785(416), or pCu-Atg9Δ766-770-GFP(416), and pAtg9Δ766-770–3HA(426), the fragment containing the indicated deletion was released from pAtg9Δ766-785-GFP(416), pAtg9Δ766-770-GFP(416), or pAtg9Δ781-785-GFP(416) by AgeI and SphI digestion and introduced into pAPG9(416), pCuAPG9GFP(416), or pAtg9-3HA(426), respectively. Point mutations in Atg9 amino acids 766–770 were introduced by site-directed mutagenesis. To construct the two-hybrid plasmid pBD-Atg9Δ766-770, the Atg9Δ766-770 fragment was amplified from pAtg9Δ766-770-GFP(416) and cloned into pGBDU-C1 using BamHI and SalI sites.

Protein A Affinity Isolation

Cells were grown to OD_{600} = 0.8 in SMD; for rapamycin treatment, cells were cultured with 0.2 μg/ml rapamycin at 30°C for an additional 2 h. Fifty milliliters of cells was harvested and resuspended in lysis buffer (20 mM Tris-HCl, pH 7.5, 150 mM KCl, 5 mM $MgCl_2$, 1% Triton X-100, 1 mM PMSF, and protease inhibitor cocktail). The detergent extracts were incubated with IgG-Sepharose beads overnight at 4°C. The beads were washed with lysis buffer six times and eluted in SDS-PAGE sample buffer by incubating at 37°C for 30 min. The eluates were resolved by SDS-PAGE and immunoblotted with anti-Atg9 antiserum or anti-HA or anti-PA antibody.

Fluorescence Microscopy

Fluorescence signals were visualized on an Olympus IX71 fluorescence microscope (Mellville, NY). The images were captured by a Photometrics CoolSNAP HQ camera (Roper Scientific, Tucson, AZ) and deconvolved using

DeltaVision software (Applied Precision, Issaquah, WA). When necessary, a mild fixation procedure was applied as previously described to visualize Atg9 without affecting various fluorescent proteins (He *et al.*, 2006).

Native Gel Analysis

Bis-Tris gels (3–12%; Invitrogen, Carlsbad, CA) were used for blue native gel electrophoresis. Spheroplasts were generated from 25 ml of cells at midlog phase as described previously (Tomashek *et al.*, 1996), and cell lysates were prepared according to the Invitrogen NativePAGE Novex Bis-Tris Gel System manual.

Tandem Affinity Purification

Four hundred milliliters of cells were cultured to OD_{600} = 0.8 in YPD. Spheroplasts were prepared and TAP purification was done as previously reported (Tomashek *et al.*, 1996; Puig *et al.*, 2001). The eluates were resolved by SDS-PAGE, and silver staining of proteins in polyacrylamide gels was performed using the SilverSNAP Stain Kit II (Thermo Scientific, Rockford, IL).

Electron Microscopy

Immunoelectron microscopy (IEM) was performed according to the procedures described previously (Baba *et al.*, 1997) with the following modifications: The blocking solution contained 0.05% Tween 20 or 0.5% cold fish gelatin (Sigma-Aldrich, St. Louis, MO). The anti-GFP (JL-8, Clontech/Takara Bio Group, Mountain View, CA) antibody was preadsorbed with a protein extract prepared from *atg9*Δ cells to reduce nonspecific staining. The secondary antibody was conjugated to Ultra Small gold particles (Aurion, Wageningen, The Netherlands) and visualized with silver enhancement.

Additional Assays

The GFP-Atg8 processing assay and the Pho8Δ60 activity assay were carried out as previously described (Abeliovich *et al.*, 2003; Shintani and Klionsky, 2004b).

RESULTS

Atg9 Self-Interacts Independent of Other Autophagy Proteins or Nutrient Status

Previously we showed that Atg9 is located at the PAS and multiple peripheral punctate sites (Reggiori *et al.*, 2004a). To determine whether Atg9 directly self-interacts, we took advantage of a new reagent, a yeast strain lacking 24 known *ATG* genes that function in *S. cerevisiae*, referred to as the multiple-knockout (MKO) strain (Cao *et al.*, 2008). Analyses by fluorescence microscopy revealed that Atg9-GFP fusion proteins were indeed organized in clusters (detected as large puncta) in this strain, as well as in the wild-type strain (Figure 1A), whereas expressing GFP alone did not lead to observable cluster formation (Supplemental Figure S1). These findings led us to propose that Atg9 may form clusters through direct self-association involving none of the other known Atg proteins. To test this hypothesis, we coexpressed Atg9 proteins fused with two different tags, GFP and DsRed, in MKO and wild-type strains. As shown in Figure 1B, the Atg9-GFP and Atg9-DsRed fusion proteins were colocalized in the cell as assessed by fluorescence microscopy.

Next, we used a biochemical coimmunoprecipitation approach to test the self-interaction of Atg9. As shown in Figure 1C, Atg9 was coprecipitated with Atg9-protein A (PA) in the MKO strain as well as in the wild-type strain in nutrient-rich conditions. As a negative control, we examined the ability of TAP-tagged Atg1 to coimmunoprecipitate Atg9-GFP; in this case, we could not examine endogenous Atg9 because of its migration at the same position as TAP-Atg1 during SDS-PAGE. In contrast to the result with Atg9-PA, Atg9-GFP was not recovered with TAP-tagged Atg1; Atg1 interacts with various other proteins including Atg13 but not Atg9, and we verified that TAP-Atg1 was able to coimmunoprecipitate Atg13 (Supplemental Figure S2A). Similarly, Atg9-PA was not able to coimmunoprecipitate Atg1 (Supplemental Figure S2B). Along with our previously published yeast two-hybrid results suggesting Atg9 self-interaction (Reggiori *et al.*, 2005), these data demonstrated that multiple Atg9 molecules were able to form a complex without any other known Atg proteins.

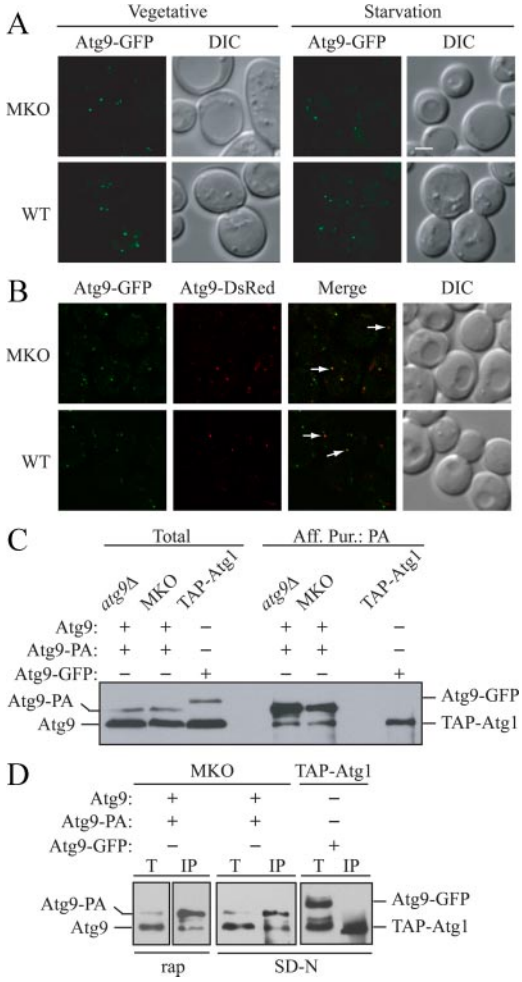

Figure 1. Atg9 self-associates independent of other Atg components or nutrient status. (A) Atg9 forms clusters independent of other Atg proteins under both nutrient-rich and nitrogen-starvation conditions. Wild-type (SEY6210; WT) or multiple-knockout (YCY123; MKO) strains were transformed with a plasmid expressing Atg9-GFP driven by the Atg9 native promoter. Cells cultured in nutrient-rich medium (Vegetative) or nitrogen-starved for 3 h (Starvation) were visualized by fluorescence microscopy. (B) Atg9 molecules colocalize. WT (CCH011) or MKO (CCH010) strains expressing integrated Atg9-3GFP and Atg9-3DsRed fusions were grown to midlog phase, subject to mild formaldehyde fixation, and imaged by fluorescence microscopy. The arrows mark examples of the sites where the two chimeras colocalize. (C) Atg9 is coprecipitated by Atg9-protein A (PA) independent of other Atg proteins. *atg9*Δ (JKY007) or MKO strains cotransformed with centromeric plasmids containing Atg9 and the Atg9-PA fusion driven by the Atg9 native promoter were used for affinity isolation. Cells were cultured in nutrient rich medium (SMD). A strain (UNY102) expressing chromosomally tagged TAP-Atg1 and plasmid-borne Atg9-GFP was used as a control in C and D. Total lysates (Total) and eluted polypeptides (Aff. Pur.) were separated by SDS-PAGE and blotted with anti-Atg9 antiserum in C and D. (D) Atg9 self-interaction in nutrient-deprived conditions is independent of other Atg components. The MKO strain expressing plasmid-borne, native promoter-driven Atg9 and Atg9-PA was used for affinity isolation. Cells were subjected to rapamycin treatment for 2 h (rap) or nitrogen starvation for 3 h (SD-N). T, total lysates; IP, immunoprecipitates. DIC, differential interference contrast. Scale bar, 2 μm.

Atg9 clustering occurs not only in nutrient-rich conditions but also during nitrogen starvation (Figure 1A). To explore

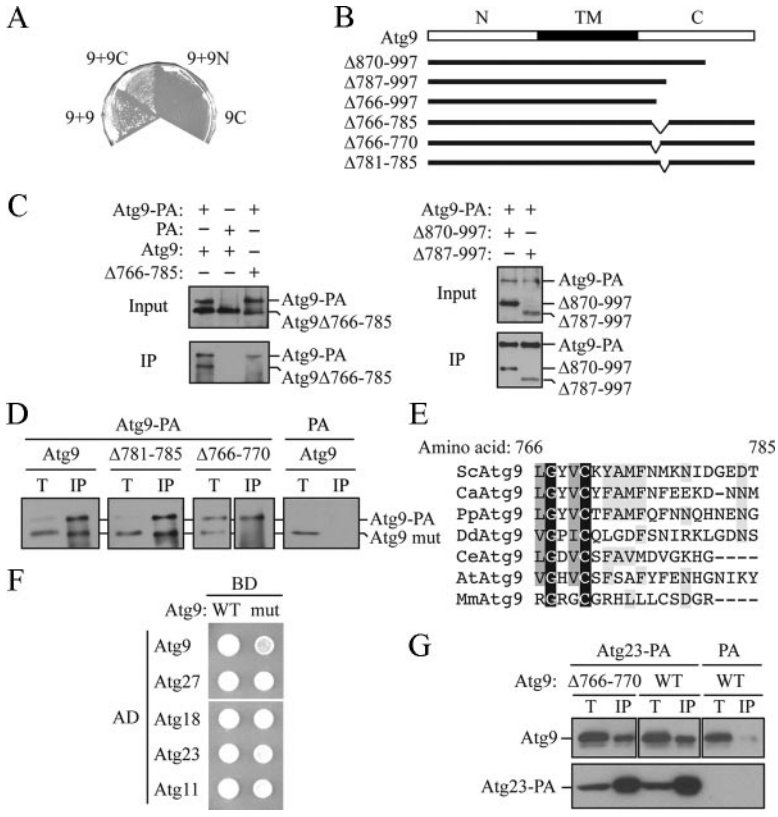

Figure 2. An Atg9 C-terminal mutant disrupts the ability to multimerize. (A) Atg9 self-interaction is mediated through its C terminus. Yeast two-hybrid cells (PJ69–4A) expressing full-length Atg9 with either full-length Atg9 (9 + 9), the Atg9 C terminus (9 + 9C) or the N terminus (9 + 9N), or expressing the Atg9 C terminus alone were grown for 6 d on plates lacking histidine. (B) Schematic representation of Atg9 truncation mutants. N, N terminus; TM, transmembrane domain; C, C terminus. (C) Atg9Δ870-997 and Atg9Δ787-997, but not Atg9Δ766-785, are coprecipitated with full-length Atg9. The MKO strain (YCY123) cotransformed with centromeric plasmids expressing native promoter-driven Atg9-PA and Atg9, Atg9Δ870-997, Atg9Δ787-997, or Atg9Δ766-785, were used for affinity isolation. Total lysates (Input) and eluted polypeptides (IP) were separated by SDS-PAGE and detected with anti-Atg9 antiserum. The MKO strain cotransformed with plasmids encoding Atg9 and PA alone was used as a control in C and D. (D) An Atg9 mutant with a five-amino acid deletion (Atg9Δ766-770) loses self-interaction. MKO cells expressing plasmid-borne Atg9-PA with Atg9, Atg9Δ781-785, or Atg9Δ766-770, driven by the Atg9 native promoter, were used for affinity isolation. (E) Alignment of Atg9 amino acids 766–785. Sequences from *S. cerevisiae*, *Candida albicans*, *Pichia pastoris*, *Dictyostelium discoideum*, *Caenorhabditis elegans*, *Arabidopsis thaliana,* and *Mus musculus* Atg9 were aligned using the ClustalW program. Amino acid identities and high and low similarities are highlighted in black, dark gray, and light gray, respectively. (F) Atg9Δ766-770 specifically loses self-interaction but not interactions with other Atg9-binding partners. The two-hybrid strain (PJ69–4A) was cotransformed with plasmids expressing the DNA-binding domain-fused wild-type Atg9 (WT) or Atg9Δ766-770 (mut) and a series of known Atg9 binding partners fused with the activation domain. Interactions were monitored by the ability of cells to grow on plates lacking histidine for 5 d. (G) Atg9Δ766-770 interacts with Atg23 similar to wild-type Atg9. An *atg9*Δ strain expressing an integrated Atg23-PA fusion (CCH020) was transformed with a 2-μm plasmid containing wild-type Atg9-triple hemagglutinin (3HA) or Atg9Δ766-770–3HA. Total lysates (T) and eluates (IP) were separated by SDS-PAGE and detected by anti-HA or anti-PA antibody. An *atg9*Δ strain expressing plasmid-borne Atg9-3HA and PA was used as a control.

whether the same Atg9 complex forms during bulk autophagy, the MKO cells were subjected to nitrogen starvation or treatment with rapamycin, a drug that partly mimics starvation conditions and induces bulk autophagy. Atg9 was coprecipitated with Atg9-PA in both conditions in the MKO strain (Figure 1D). As before, Atg9-GFP was not coisolated with TAP-tagged Atg1. Similar results were obtained using wild-type cells (Supplemental Figure S2C). In addition, we found that Atg9 self-interaction is enhanced during starvation, based on quantification of the relative Atg9 amount precipitated by Atg9-PA (Supplemental Figure S2D), implicating an important role of self-interaction during autophagosome formation. Collectively, we concluded that Atg9 self-interacts independent of any other known Atg proteins in both nutrient-rich and starvation conditions, which may correlate with a role for Atg9 in both selective and nonselective bulk autophagy.

An Atg9 C-Terminal Mutant Disrupts Its Ability to Multimerize

Next, we wanted to study the physiological function of Atg9 self-interaction in autophagy. Accordingly, we first mapped the interaction domain by the yeast two-hybrid approach. In the presence of full-length Atg9, the Atg9 C-terminal domain supported the growth of two-hybrid cells on selective plates lacking histidine as well as full-length Atg9, whereas the N terminus was not able to do so (Figure 2A), indicating that Atg9 self-interaction is mediated through the C terminus. To narrow down the critical region, we further constructed a series of Atg9 C-terminal deletion mutants (Figure 2B) and analyzed them using the coimmunoprecipitation assay. Atg9, Atg9Δ870-997, and Atg9Δ787-997, but not Atg9Δ766-785 or Atg9Δ766-997, were pulled down by full-length Atg9-PA (Figure 2C and unpublished data), suggesting that amino acids included in the region of 766–786 were required for self-interaction. Atg9 and the PA vector were coexpressed as a control and no detectable Atg9 was coprecipitated by PA. On the basis of this result, we generated four additional mutants each lacking five consecutive amino acids within the sequence of amino acids 766–786. By coimmunoprecipitation assays we determined that Atg9Δ766-770 was unable to interact with Atg9, whereas the other mutants displayed a normal interaction (Figure 2D and unpublished data). We note that amino acids 766–770 are highly conserved through evolution (Figure 2E).

Because Atg9 interacts with several other known Atg proteins, we further tested the ability of Atg9Δ766-770 to bind these other binding partners by yeast two-hybrid assays. Although Atg9Δ766-770 had a significantly compromised interaction with Atg9, it was still able to bind to its other binding partners, including Atg23, Atg27, Atg18, and Atg11, with apparently normal affinity (Figure 2F). In addition, we verified that the interaction between Atg9Δ766-770 and Atg23 was not impaired based on coimmunoprecipitation; we used a vector expressing PA alone as a negative control (Figure 2G). Therefore, the C-terminal mutant

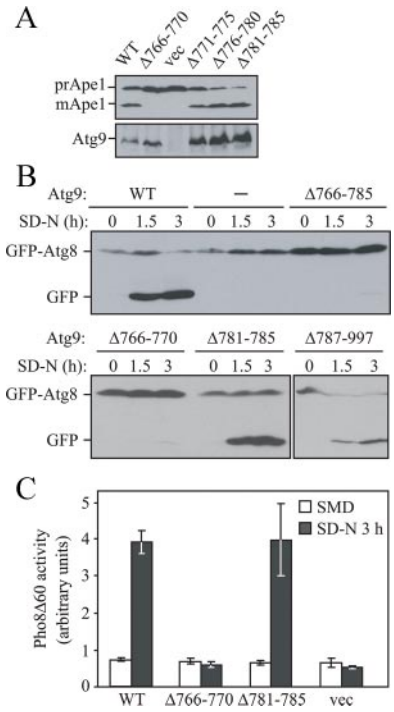

Figure 3. Atg9 self-interaction is required for autophagy activity in both nutrient-rich and starvation conditions. (A) Precursor Ape1 maturation is blocked in cells expressing Atg9Δ766-770. An *atg9*Δ strain (JKY007) was transformed with an empty vector, or a plasmid expressing wild-type Atg9 or a series of truncation mutants (Δ766-770, Δ771-775, Δ776-780, and Δ781-785) driven by the Atg9 native promoter. Protein extracts were analyzed by Western blotting using antiserum to Ape1 or Atg9. (B) GFP-Atg8 processing is impaired by deletion of residues 766–770 of Atg9. The *atg9*Δ strain (JKY007) was cotransformed with a GFP-Atg8 plasmid and an empty vector (−), or a plasmid expressing wild-type Atg9 or a series of truncation mutants (Δ766-785, Δ766-770, Δ781-785, and Δ787-997). Cells were grown in nutrient-rich medium to midlog phase then shifted to nitrogen-starvation conditions (SD-N). Aliquots were taken at the indicated time points and analyzed by Western blotting using anti-GFP antibody. (C) Pho8Δ60 activity is reduced in Atg9Δ766-770-expressing cells. The *atg9*Δ strain (CCH002) transformed with a plasmid expressing native promoter-driven wild-type Atg9 (WT), Atg9Δ766-770, Atg9Δ781-785, or an empty vector (vec), were grown in nutrient-rich medium (SMD) to midlog phase then shifted to starvation medium (SD-N) for 3 h. The Pho8Δ60 activity was measured according to *Materials and Methods.* Error bars, SD of three independent experiments.

Atg9Δ766-770 specifically disrupts the self-interaction of Atg9 and was used for the following functional analyses.

Atg9 Self-Interaction Is Required for Autophagy Progression

To study the function of Atg9 self-interaction in autophagy, we adopted several established assays using the Atg9Δ766–770 mutant. The processing of prApe1 into mature Ape1 results in a migration shift during SDS-PAGE and can be monitored as an indicator for selective autophagy. As shown in Figure 3A, Atg9Δ766-770, which impaired the self-interaction of Atg9, blocked the maturation of prApe1, whereas the other three deletion mutants, which had no effect on Atg9 self-interaction, retained the capacity of prApe1 maturation similar to wild-type Atg9, although all of the Atg9 mutants displayed a level of stability at least equivalent to that of the wild-type protein. This indicated that the self-interaction of Atg9 is indispensable for selective autophagy.

We also observed that Atg9 self-interaction occurs under nitrogen-starvation conditions, which suggests that a protein complex containing multiple Atg9 proteins may be involved in bulk autophagy. To test this hypothesis, we carried out two assays to measure bulk autophagy activity when Atg9 self-interaction was altered. Atg8 is conjugated to phosphatidylethanolamine (PE) and remains associated with the completed autophagosome and thus is a marker for autophagy progression (Kirisako *et al.*, 1999; Huang *et al.*, 2000). During autophagy, the GFP-tagged Atg8 is transported to the vacuole where Atg8 is rapidly degraded, whereas the GFP moiety remains relatively stable. Thus, the accumulation of free GFP detected by Western blot reflects autophagy activity (Shintani and Klionsky, 2004b). We assayed GFP-Atg8 processing with the mutants mentioned above and found that only with Atg9Δ766-770 and Atg9Δ766-785, both of which affected Atg9 self-interaction (Figure 2D and unpublished data), GFP-Atg8 processing was blocked. With two other mutants Atg9Δ781-785 and Atg9Δ787-997 that did not affect Atg9 self-interaction, GFP-Atg8 was processed similar to cells expressing wild-type Atg9 (Figure 3B). These data demonstrated that loss of Atg9 self-interaction caused a defect in bulk autophagy. To quantitatively confirm this result, we measured the Pho8Δ60 enzymatic activity. Pho8Δ60 is a truncated form of alkaline phosphatase that can be delivered to the vacuole only via autophagy (Noda *et al.*, 1995). Approximately fourfold induction of Pho8Δ60 activity by starvation was observed with wild-type Atg9 and Atg9Δ781-785, whereas the empty vector and Atg9Δ766-770 showed only the basal level of Pho8Δ60 activity (Figure 3C). We further introduced alanine mutations at each conserved residue (Figure 2E) in the region 766–770, and found that these mutations also caused defects in the Cvt pathway and bulk autophagy (Table 2). Thus, even point mutations in the highly conserved interaction domain interfere with Atg9 function. Taken together, these results indicate that Atg9 self-interaction is also functionally essential for bulk autophagy. Thus our data revealed a previously unknown mechanism of Atg9 shared in both selective and bulk autophagy, involving formation of a multiple Atg9-containing complex that depends on interaction between Atg9 proteins.

Table 2. Point mutations to alanine in Atg9 amino acids 766–770 affect autophagy

	Cvt	Autophagy
LGYVC	+	+
L to A	−	−
G to A	−	−
V to A	−	−
C to A	−	+/−
V to A C to A	−	−

−, complete block; +/−, partial block.

Self-Interaction Promotes Anterograde Transport of Atg9 and Formation of Intact Phagophores

We decided to investigate the underlying mechanisms of the functional defects seen with the Atg9Δ766-770 mutant. In the absence of Atg9, a number of Atg proteins are not correctly localized to the PAS, including Atg2, Atg14, and Atg18 (Suzuki *et al.*, 2001). Therefore it is possible that formation of

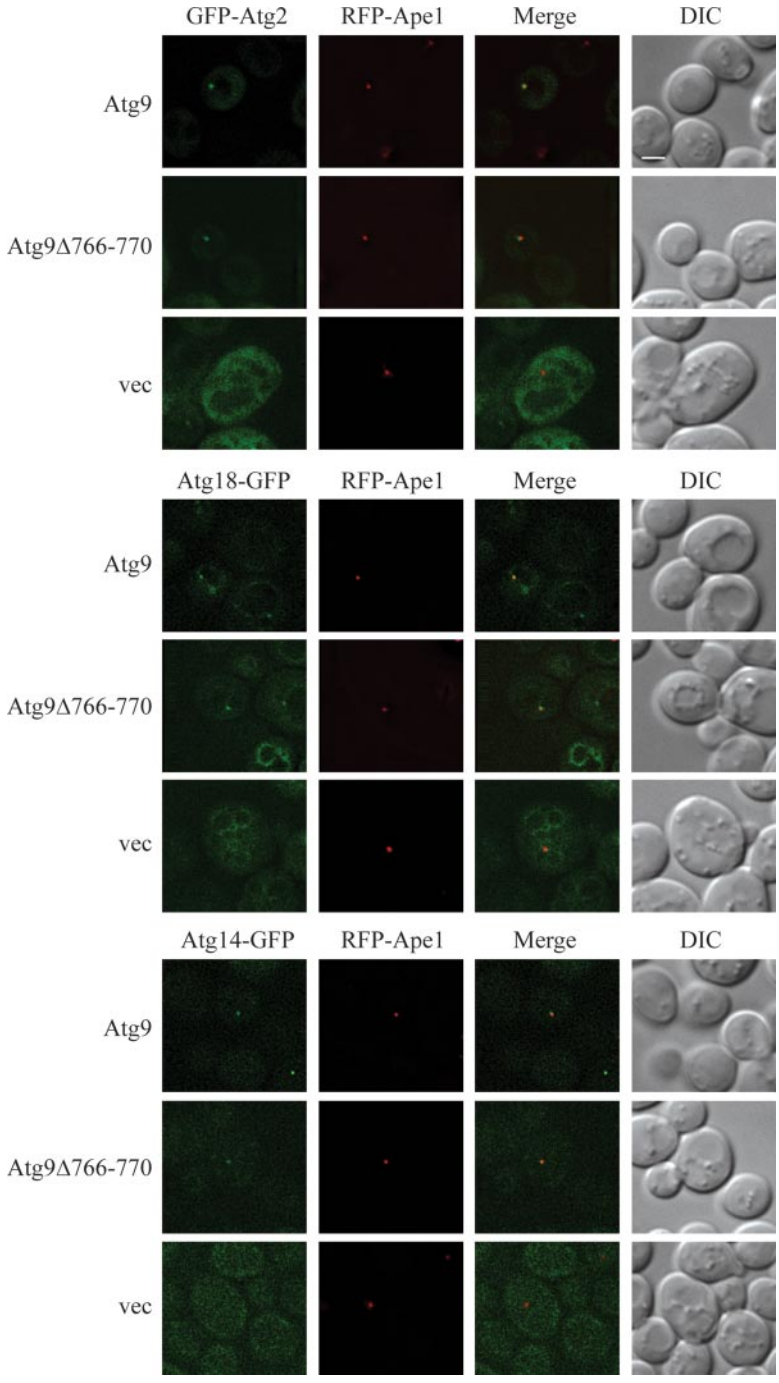

Figure 4. Atg9Δ766–770 is not defective in the PAS recruitment of other Atg proteins. An *atg9*Δ strain expressing integrated RFP-Ape1 (CCH025) was co-transformed with a plasmid expressing either *CUP1* promoter-driven GFP-Atg2 or native *ATG18* promoter-driven Atg18-GFP and a 2-micron plasmid expressing wild-type Atg9, Atg9Δ766-770, or an empty vector. An *atg9*Δ strain expressing chromosomally tagged Atg14-GFP and RFP-Ape1 (CCH026) was transformed with the above 2-μm plasmid expressing wild-type Atg9, Atg9Δ766-770, or an empty vector. Cells were cultured in nutrient-rich medium to midlog phase and imaged by fluorescence microscopy. DIC, differential interference contrast. Scale bar, 2 μm.

a multimeric Atg9 complex is required for recruitment of these proteins to the PAS. To examine this possibility, we visualized the localization of Atg2, Atg18, and Atg14 in cells expressing wild-type Atg9 or Atg9Δ766-770. As shown in Figure 4, in the presence of either wild-type Atg9 or Atg9Δ766-770, Atg2, Atg18, and Atg14 localized to a primary perivacuolar punctum, which colocalized with RFP-Ape1 and corresponded to the PAS. These data suggested that PAS recruitment of Atg proteins by Atg9Δ766-770 was not affected and thus was not the causal factor for the autophagy deficiencies.

We then hypothesized that the self-interaction may be involved in the trafficking of Atg9. According to the "cycling" model of Atg9 transport, when the retrograde transport of Atg9 is impaired, Atg9 will accumulate at the PAS as one primary punctum (Reggiori *et al.*, 2004a), but this accumulation was not observed with Atg9Δ766-770 in otherwise wild-type yeast cells; besides, Atg9Δ766-770 partially colocalized with mitochondria similar to wild-type Atg9 (unpublished data). Thus, Atg9 self-interaction is unlikely to be involved in the retrograde trafficking of Atg9 back to the peripheral (i.e., non-PAS) sites. Accordingly, to study whether self-interaction is involved in Atg9 anterograde transport, we used the TAKA (transport of Atg9 after knocking out *ATG1*) assay (Cheong *et al.*, 2005). Atg1 is a key regulator that activates the retrieval of Atg9 from the

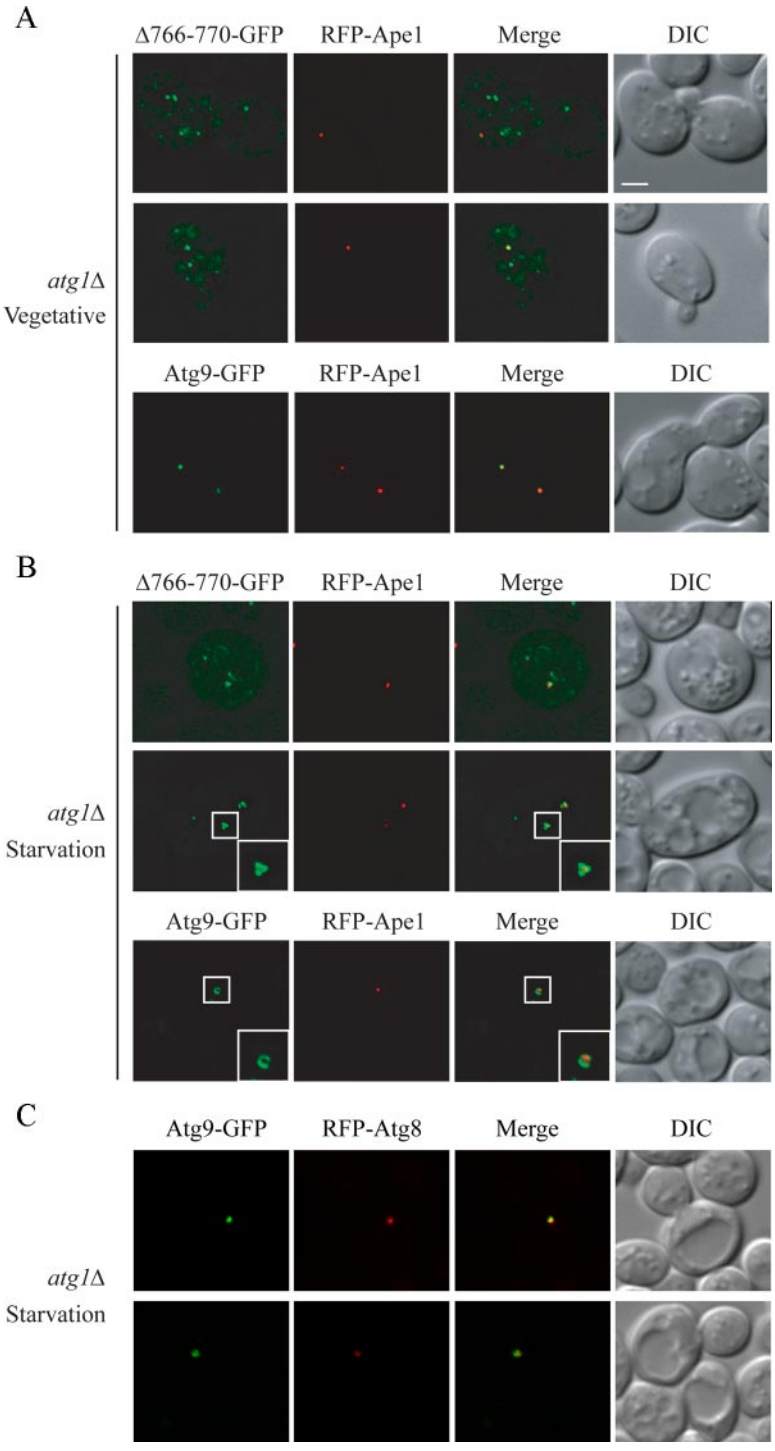

Figure 5. Atg9Δ766-770 is defective in PAS targeting and phagophore formation. (A) Atg9Δ766-770 has a partial defect in anterograde transport from peripheral sites to the PAS during growth. The *atg1*Δ *atg9*Δ strain (CCH001) was cotransformed with a RFP-Ape1 plasmid and a plasmid expressing wild-type Atg9-GFP or Atg9Δ766-770-GFP driven by the *CUP1* promoter. Cells were cultured in nutrient-rich medium to midlog phase and imaged by fluorescence microcopy. (B) Atg9Δ766-770 forms an abnormal fragmented phagophore. The cells in A were cultured to midlog phase and subject to nitrogen starvation for 3 h before imaging by fluorescence microscopy. Bottom right panels are enlarged images of the boxed regions. (C) The phagophore is colabeled with Atg9 and Atg8. The *atg1*Δ *atg9*Δ strain (CCH001) was cotransformed with plasmids expressing Atg9-GFP and RFP-Atg8. Cells were cultured to midlog phase and subject to nitrogen starvation for 2 h before imaging by fluorescence microscopy. DIC, differential interference contrast. Scale bar, 2 μm.

PAS to the peripheral sites and deleting *ATG1* restricts Atg9 to the PAS. The TAKA assay examines the epistasis of a second mutation relative to *atg1*Δ with regard to Atg9 localization at the PAS. Using fluorescence microscopy, we imaged the localization of Atg9Δ766-770-GFP and wild-type Atg9-GFP in *atg1*Δ cells in nutrient-rich and starvation conditions.

As shown in Figure 5A, in contrast to wild-type Atg9, which was restricted to the PAS (marked with RFP-Ape1) in 87% (52/60) of the cells, the Atg9Δ766–770 mutant distributed to multiple punctate or dispersed structures, in addition to the PAS location in 70% (52/74) of the cells. Such localization was observed regardless of nutrient supply (Figure 5B). During nitrogen starvation, in 53% (23/43) of the *atg1*Δ cells, Atg9Δ766-770 localized to multiple puncta, compared with only 11% (12/107) of the cells displaying peripheral localization with wild-type Atg9. Thus, these results demonstrated that loss of Atg9 self-interaction partially blocked the anterograde trafficking of Atg9 to the PAS during selective and bulk autophagy. Self-interacting and forming a complex could concentrate Atg9 molecules as clusters at the peripheral compartments, which may be important for

efficient trafficking of Atg9 from these sites for subsequent delivery to the PAS.

On nutrient deprivation, formation of a continuous cup-shaped or ring-like structure by wild-type Atg9-GFP was visualized around the cargo prApe1 at the PAS and colabeled with Atg8 by fluorescence microscopy (Figure 5, B and C), suggesting that they were authentic phagophores. These structures were difficult to detect in wild-type cells, presumably because of their transient nature and the rapid dissociation of Atg9 from them upon autophagosome completion. Previous studies, however, show that autophagosomes emerge from Atg8-labeled intermediates in *atg1* temperature-sensitive cells, indicating that in this mutant these are not dead-end structures (Suzuki *et al.*, 2001). The cup-shaped structures were ~500 nm in diameter, which fits within the size range of completed autophagosomes in yeast (400–900 nm; Takeshige *et al.*, 1992). Together, these data suggested that the expanding phagophore (or precursor membrane of the phagophore) is an Atg9-containing intermediate. Additionally, the Atg9-containing structures were seen with various sizes and curvatures (Supplemental Figure S3), which may represent different expansion stages of the phagophore. Nonetheless, we cannot definitively conclude that the structures accumulating in the *atg1*Δ mutant are authentic phagophores, and in particular the size may appear exaggerated by fluorescence microscopy because of the accumulation of Atg9-GFP as a result of the *ATG1* deletion. With this caution in mind, we refer to the Atg9-containing structure as the phagophore for simplicity.

Interestingly, the phagophore structure was fragmented and/or failed to elongate normally when Atg9Δ766-770-GFP replaced the wild-type Atg9-GFP (Figure 5B). To further characterize the Atg9-containing structures at the PAS at a higher resolution, we applied IEM. Atg9-GFP or Atg9Δ766-770-GFP was expressed in an *atg1*Δ *atg9*Δ strain, and the Atg9 protein was detected with anti-GFP antibody. As previously reported (Baba *et al.*, 1997), the Cvt complex formed by prApe1 and its receptor Atg19 was localized as a spherical electron-dense particle usually near the vacuole. Consistent with our result by fluorescence microscopy, wild-type Atg9 gold particles (arrows) were concentrated on the surface of membranous structures (arrowheads) surrounding the Cvt complex, whereas the Atg9Δ766-770 mutant that lost self-interaction appeared less clustered at the PAS (Figure 6, A and B). In sections prepared by freeze substitution but not immunostained, the membrane structures were more readily detected. In this case, it appeared that there were more membranes, potentially corresponding to the phagophore, surrounding the Cvt complex in wild-type cells relative to the Atg9Δ766-770 mutant. This result suggests that Atg9 self-interaction may be required to foster expansion of, or maintain the integrity of, the phagophore at the PAS.

To quantitatively analyze this difference, we further counted the average number of wild-type or mutant Atg9 molecules around the Cvt complex. As shown in Figure 6C, the molecule number of Atg9Δ766-770 per Cvt complex was markedly reduced compared with wild-type Atg9, suggesting that Atg9 self-association is essential for efficient delivery to the PAS. On the basis of these data and our previous Atg9 cycling model, we propose that an Atg9 complex is dependent on its self-interaction and that the complex formation may facilitate not only the flow of membrane to the PAS but also the fusion of small membrane fragments into a continuous larger phagophore to form an autophagosome.

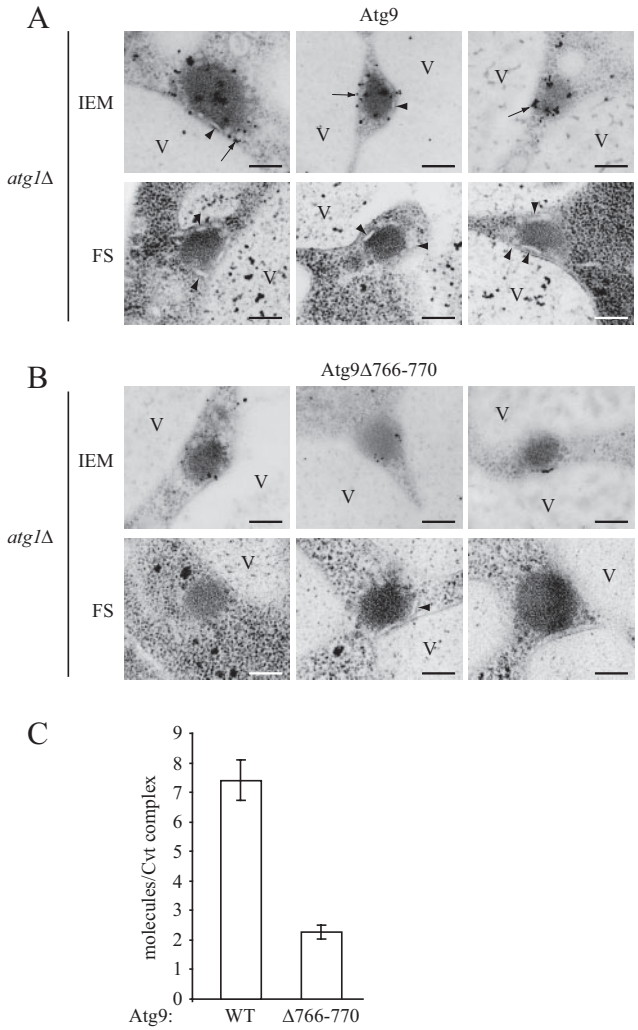

Figure 6. Atg9 localizes to the phagophore structure surrounding the Cvt complex. (A and B) The *atg1*Δ *atg9*Δ strain was transformed with a plasmid expressing *CUP1* promoter-driven Atg9-GFP (A) or Atg9Δ766-770-GFP (B). Cells were grown to midlog phase, shifted to SD-N for 3 h, and prepared for electron microscopy using freeze substitution (FS) and stained with anti-GFP antibody followed by immunogold as indicated (IEM). Representative images are shown. Arrows mark Atg9 and membranous structures enwrapping the Cvt complex are indicated by arrowheads. V, vacuole. (C) The number of Atg9 or Atg9Δ766-770 molecules around Cvt complexes was quantified based on IEM images shown in A and B. $n = 100$; $p < 0.0001$. Error bars, SEM and statistical significance was analyzed by Student's two-tailed *t* test. Scale bar, 200 nm.

The Ability to Multimerize Is Required for Atg9 Function at the PAS

Because Atg9Δ766-770 partially affected the anterograde trafficking of Atg9 to the PAS, it is possible that the abnormal phagophore structure we observed with Atg9Δ766-770 is due to insufficient supply of this protein to the PAS. To test this possibility, we relied on the overexpression of Atg11, which increases the anterograde transport of Atg9 to the PAS (He *et al.*, 2006). We imaged the GFP-tagged Atg9 and CFP-tagged Atg11 pairs with a yellow fluorescent protein (YFP)/CFP filter set by fluorescence microscopy, and, as reported previously (Kaksonen *et al.*, 2003), no detectable bleed-through of the GFP signal from the CFP filter was seen. Because Atg9Δ766-770 did not affect its interaction

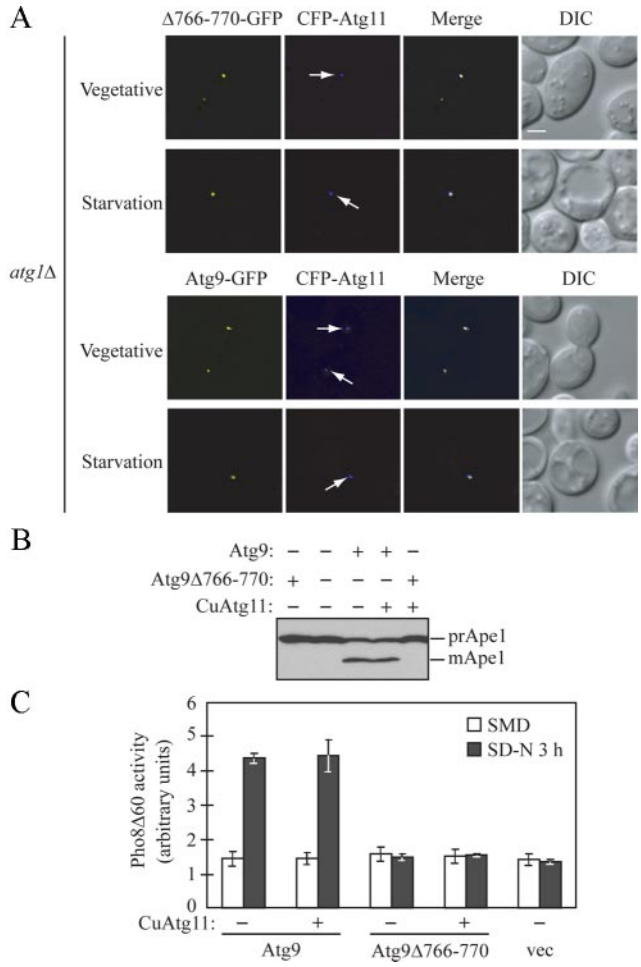

Figure 7. Atg9 functions in an oligomeric state at the PAS. (A) Overexpression of Atg11 rescues Atg9Δ766-770 transport to the PAS in both nutrient-rich and starvation conditions. The *atg1*Δ *atg9*Δ strain (CCH001) was cotransformed with centromeric plasmids containing *CUP1* promoter-driven CFP-Atg11 and wild-type Atg9-GFP, or Atg9Δ766-770-GFP. Cells were cultured in nutrient-rich medium to midlog phase and imaged by fluorescence microscopy (Vegetative) or were shifted to starvation medium for 3 h before microscopy imaging (Starvation). DIC, differential interference contrast. Scale bar, 2 μm. (B) Atg11 overexpression does not rescue the Cvt pathway in cells expressing Atg9Δ766-770. The *atg9*Δ strain (JKY007) expressing plasmid-borne wild-type Atg9 or Atg9Δ766-770, with or without *CUP1* promoter-driven Atg11, were grown to midlog phase, and protein extracts were analyzed by Western blotting using anti-Ape1 antiserum. (C) Atg11 overexpression does not rescue Atg9Δ766–770 function in bulk autophagy. The *atg9*Δ strain (CCH002) expressing plasmid-borne *CUP1* promoter-driven wild-type Atg9 or Atg9Δ766-770, or an empty vector (vec), with or without *CUP1* promoter-driven Atg11, were grown in SMD to midlog phase and shifted to SD-N for 3 h. The Pho8Δ60 activity was measured according to *Materials and Methods.* Error bars, SD of three independent experiments.

with Atg11 (Figure 2F), we were able to overcome the inefficient anterograde transport of Atg9Δ766-770 to the PAS by overexpressing Atg11 in both *atg1*Δ and wild-type cells (Figure 7A and unpublished data), such that in nutrient-rich conditions the subcellular localization of Atg9Δ766-770 (68%; 36/53 cells) basically was indistinguishable from wild-type Atg9 (84%; 48/57 cells). The transport restoration was also observed in starvation conditions (Figure 7A; 73% of Atg9Δ766-770 cells [36/49] and 84% of wild-type Atg9 cells [46/55]). This phenotype indicates that the deletion of residues 766–770 did not absolutely block the ability of Atg9 to transit to the PAS and rules out accumulation in the endoplasmic reticulum due to protein misfolding as the cause of the functional defect. The increase in PAS localization of Atg9Δ766-770, however, did not result in the maturation of prApe1, indicating that this type of selective autophagy was still defective (Figure 7B). The Pho8Δ60 activity assay also showed that bulk autophagy was not rescued by enhancing the anterograde flow of the mutant Atg9 (Figure 7C). In either case, the overexpression of Atg11 did not interfere with the function of wild-type Atg9, indicating that this level of Atg11 did not cause a dominant negative phenotype. Therefore, these results clearly suggested that a normal multimeric state or the ability to multimerize is essential for Atg9 function after it reaches the PAS, which is a critical step during phagophore formation.

To further investigate the nature of the Atg9 complex, we performed a native gel analysis using the MKO strain expressing wild-type Atg9 or the mutant. We discovered that Atg9Δ766-770 migrated faster than wild-type Atg9 in native conditions (Figure 8A). As a control, we examined the dodecamer complex assembled by prApe1 (Kim *et al.*, 1997) and found that it remained intact, suggesting that Atg9Δ766-770 was not able to form complexes as large (or as stable) as those seen with the wild-type protein. Consistent with the previous results showing that overexpression of Atg11 did not rescue the functional defect of the Atg9Δ766-770 mutant (Figure 7B), overexpression of Atg11 did not rescue the defect in complex formation of Atg9Δ766-770 in native conditions (Figure 8B). We further analyzed the Atg9 complex size in the wild-type background, by expressing wild-type or mutant Atg9 in the *atg9*Δ strain. As shown in Figure 8C, both wild-type and mutant Atg9 displayed similar migration patterns as in the MKO cells, suggesting that the known Atg9 interaction partners among Atg proteins may be dynamically associated with Atg9, rather than stably present in the core Atg9 complex. In addition, consistent with Figure 1 and Supplemental Figure S2, we also detected that the Atg9 complex remained intact upon rapamycin treatment (Figure 8C).

We noticed that Atg9Δ766-770 did not migrate as a monomer (~150 kDa on native gels, unpublished data), but ran at a position that might correspond to a tetramer. This might reflect the fact that the mutant only partially impaired Atg9 complex formation as suggested by a compromised, but not complete loss of, interaction seen by the yeast two-hybrid assay (Figure 2F), but it is also possible that the Atg9 complex contains unknown protein components as potential regulators of Atg9 function. To distinguish between these two possibilities, we performed a native purification of the Atg9 complex by the TAP method. We generated a strain expressing the chromosomally tagged Atg9-TAP fusion and another strain expressing the TAP tag alone integrated immediately after the *ATG9* promoter as a control. The TAP tag was cleaved from Atg9-TAP after the first immunoprecipitation by IgG Sepharose, and the Atg9 complex was isolated by a second immunoprecipitation with calmodulin affinity resin. The proteins precipitated by Atg9 were analyzed on SDS-PAGE gels and detected by silver stain. Besides Atg9 (at the size of ~130 kDa), four major protein bands were detected at ~94, 54, 28, and 25 kDa, compared with the control (Figure 8D), suggesting that the Atg9 complex is actually composed of multiple proteins, although we cannot rule out at present that these represent degradation products. It will be helpful to further study the identity and function of these components in the Atg9 complex during phagophore formation and expansion.

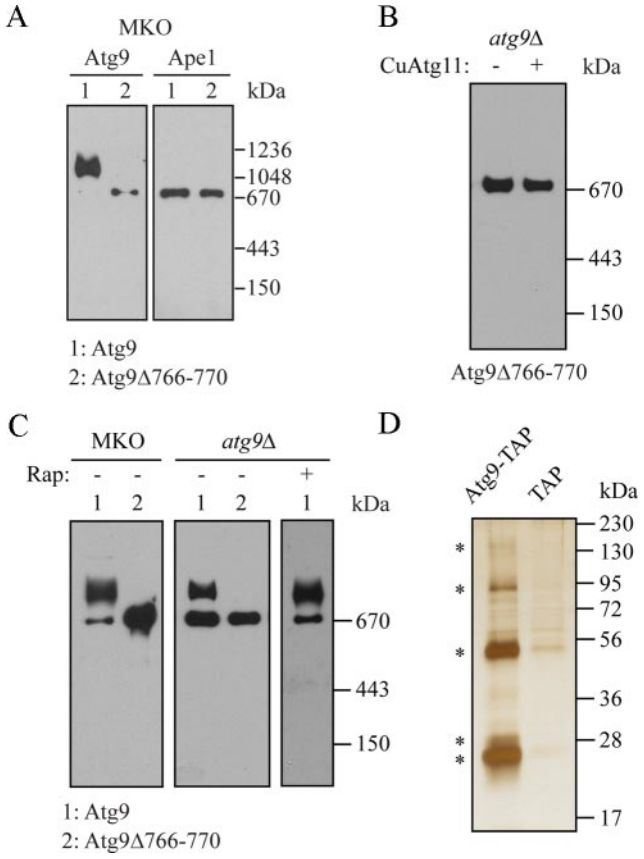

Figure 8. Biochemical characterization of the Atg9-containing complex. (A) Atg9Δ766-770 forms smaller complexes than wild-type Atg9 in the MKO strain. The MKO strain (YCY123) was transformed with a 2-μm plasmid expressing wild-type Atg9 or Atg9Δ766-770. Cell lysates were prepared under native conditions as described in *Materials and Methods* and analyzed on native gels in A–C. (B) Atg11 overexpression does not rescue the defect in complex formation resulting from Atg9 loss of self-interaction. The *atg9*Δ strain was cotransformed with plasmids expressing *CUP1* promoter-driven HA-Atg11 and Atg9Δ766-770 as indicated. (C) Atg9 forms stable complexes in the wild-type strain during starvation. The MKO (YCY123) or *atg9*Δ (JKY007) strain was transformed with a 2-μm plasmid expressing wild-type Atg9 or Atg9Δ766-770. Cells were grown in SMD to midlog phase and treated with rapamycin for an additional 1.5 h if indicated. Native gels are detected with antiserum to Atg9 or Ape1 in A, and with Atg9 antiserum in B and C. (D) The Atg9 complex contains five different proteins. Two strains expressing the chromosomally tagged Atg9-TAP (CCH019) or an integrated TAP tag alone driven by the *ATG9* promoter (CCH027) were used in tandem affinity purification as described in *Materials and Methods.* The eluates were analyzed on 10% SDS-PAGE gels and detected by silver staining. Proteins coprecipitated with Atg9 are marked by asterisks.

DISCUSSION

Atg9 is the only known integral membrane protein that is required in the formation of sequestering vesicles during all types of autophagy, including the Cvt pathway, pexophagy, mitophagy (Kanki and Klionsky, 2008) and bulk autophagy, and it may play a key role in lipid delivery to the PAS. In addition to the PAS, Atg9 is localized at cytoplasmic punctate structures, which undergo dynamic movement revealed by time-lapse microscopy (Reggiori *et al.,* 2005). Our data indicate that the clustered organization of Atg9 may be mediated by the ability to self-interact. We also found that self-interaction is important for efficient anterograde transport of Atg9 to the PAS (Figure 5). It is possible that Atg9 multimerization as clusters may function in promoting membrane "budding," although the mechanism that triggers Atg9 movement from the peripheral compartments is not clear.

Our microscopy analyses revealed for the first time that Atg9 is localized on the membrane structures enwrapping the Cvt complex at the PAS, and thus we suggest that Atg9 can be used as a marker for monitoring phagophore expansion, although the PAS in the *atg1*Δ mutant represents a relatively static structure compared with the authentic phagophore in wild-type cells. Also, we do note that we cannot unequivocally identify the apparent membrane fragments as belonging to the phagophore because we did not carry out dual immunolabeling with anti-Atg8, which is known to localize to the PAS in the *atg1*Δ strain. We speculate that the precise regulation of Atg9 self-interaction may facilitate tethering and fusion of small membranes at the PAS. Notably, no yeast SNAREs (*N*-ethylmaleimide-sensitive factor attachment protein receptor) have yet been localized to the PAS (Reggiori *et al.,* 2004b), implying that membrane fusion at, and closure of, the phagophore may adopt a mechanism different from the conventional SNARE-mediated manner, although it is possible that SNAREs are present at too low a level to detect by fluorescence microscopy. Recent studies suggest that lipidated Atg8–PE mediates membrane hemifusion of liposomes in vitro (Nakatogawa *et al.,* 2007). Yet, how Atg8 leads to membrane hemifusion in vivo and how hemifusion of lipid bilayers contributes to phagophore expansion is not clear. A recent analysis of Atg8 function suggests that Atg8 may largely determine the autophagosome size, but not the biogenesis of the initial phagophore or its completion (Xie *et al.,* 2008). As suggested in this study, it is possible that Atg9 plays a critical role in initiating the phagophore. Furthermore, Atg9 along with Atg8–PE, and other Atg proteins, actively participate in the fusion process that expands the phagophore into the autophagosome. However, as noted above, it is not yet known whether Atg8–PE is present on the Atg9-containing membrane segments that are involved in autophagosome biogenesis.

It should be noted that the cup-shaped phagophore is formed in cells lacking Atg1 (Figures 5B, 6, A and B, and Supplemental Figure S3). Thus the Atg1 kinase, originally proposed to function in phagophore initiation, appears to be dispensable for this process. In addition, both Atg2 and Atg18 are absent from the PAS in *atg1*Δ cells (Suzuki *et al.,* 2007). Therefore, the cup-shaped phagophore we observed around prApe1 seems to form independently of Atg1, Atg2, and Atg18. Given the previous reports showing that the absence of any of these three proteins causes accumulation of Atg9 at the PAS (Reggiori *et al.,* 2004a), it would be reasonable to hypothesize that Atg1, Atg2, and Atg18 function at the vesicle completion step and promote dissociation of Atg9 after vesicle sealing, and lacking any of them will arrest the phagophore as an intermediate structure. Notably, Atg1 also seems to function at a late stage and is not required for induction of micropexophagy in the methylotrophic yeast *Pichia pastoris* (Mukaiyama *et al.,* 2002). Thus, the protein machinery responsible for autophagy induction, and the exact role of Atg1, remain to be further elucidated.

The MKO strain allowed us to investigate the formation of the Atg9 complex bypassing the complexity caused by multiple Atg9-binding partners among Atg proteins. Using Atg9 as a phagophore marker, the MKO strain will provide advantages for studying proteins required in distinct steps during autophagosome formation including nucleation, expansion, and completion of the sequestering vesicle. We found that additional proteins may be stably present in the Atg9 complex

(Figure 8D), and it is possible that they function as regulatory units. It will be interesting to further characterize these members of the Atg9 complex for a better understanding of membrane dynamics during de novo autophagosome biogenesis.

ACKNOWLEDGMENTS

The authors thank Dr. Fulvio Reggiori (University Medical Centre Utrecht) for providing the pS1S2(416) plasmid, Dr. Noriko Nagata (Japan Women's University) for the use of the electron microscopy facilities, members of the Klionsky lab for valuable comments and suggestions to this project, and Drs. Weibin Zhou and Clinton Bartholomew for critical reading of the manuscript. This work is supported by a Rackham Predoctoral Fellowship to C.H. and National Institutes of Health Public Health Service Grant GM53396 to D.J.K.

REFERENCES

Abeliovich, H., Zhang, C., Dunn, W. A., Jr., Shokat, K. M., and Klionsky, D. J. (2003). Chemical genetic analysis of Apg1 reveals a non-kinase role in the induction of autophagy. Mol. Biol. Cell *14*, 477–490.

Baba, M., Osumi, M., Scott, S. V., Klionsky, D. J., and Ohsumi, Y. (1997). Two distinct pathways for targeting proteins from the cytoplasm to the vacuole/lysosome. J. Cell Biol. *139*, 1687–1695.

Cao, Y., Cheong, H., Song, H., and Klionsky, D. J. (2008). *In vivo* reconstitution of autophagy in *Saccharomyces cerevisiae.* J. Cell Biol., *182*, 703–713.

Cheong, H., Nair, U., Geng, J., and Klionsky, D. J. (2008). The Atg1 kinase complex is involved in the regulation of protein recruitment to initiate sequestering vesicle formation for nonspecific autophagy in *Saccharomyces cerevisiae.* Mol. Biol. Cell *19*, 668–681.

Cheong, H., Yorimitsu, T., Reggiori, F., Legakis, J. E., Wang, C.-W., and Klionsky, D. J. (2005). Atg17 regulates the magnitude of the autophagic response. Mol. Biol. Cell *16*, 3438–3453.

Guan, J., Stromhaug, P. E., George, M. D., Habibzadegah-Tari, P., Bevan, A., Dunn, W. A., Jr., and Klionsky, D. J. (2001). Cvt18/Gsa12 is required for cytoplasm-to-vacuole transport, pexophagy, and autophagy in *Saccharomyces cerevisiae* and *Pichia pastoris.* Mol. Biol. Cell *12*, 3821–3838.

He, C., Song, H., Yorimitsu, T., Monastyrska, I., Yen, W.-L., Legakis, J. E., and Klionsky, D. J. (2006). Recruitment of Atg9 to the preautophagosomal structure by Atg11 is essential for selective autophagy in budding yeast. J. Cell Biol. *175*, 925–935.

Huang, W.-P., Scott, S. V., Kim, J., and Klionsky, D. J. (2000). The itinerary of a vesicle component, Aut7p/Cvt5p, terminates in the yeast vacuole via the autophagy/Cvt pathways. J. Biol. Chem. *275*, 5845–5851.

James, P., Halladay, J., and Craig, E. A. (1996). Genomic libraries and a host strain designed for highly efficient two-hybrid selection in yeast. Genetics *144*, 1425–1436.

Kaksonen, M., Sun, Y., and Drubin, D. G. (2003). A pathway for association of receptors, adaptors, and actin during endocytic internalization. Cell *115*, 475–487.

Kanki, T., and Klionsky, D. J. (2008). Mitophagy in yeast occurs through a selective mechanism. J. Biol. Chem. *283*, (*in press*).

Kim, J., Huang, W.-P., Stromhaug, P. E., and Klionsky, D. J. (2002). Convergence of multiple autophagy and cytoplasm to vacuole targeting components to a perivacuolar membrane compartment prior to *de novo* vesicle formation. J. Biol. Chem. *277*, 763–773.

Kim, J., Kamada, Y., Stromhaug, P. E., Guan, J., Hefner-Gravink, A., Baba, M., Scott, S. V., Ohsumi, Y., Dunn, W. A., Jr., and Klionsky, D. J. (2001). Cvt9/Gsa9 functions in sequestering selective cytosolic cargo destined for the vacuole. J. Cell Biol. 153, 381–396.

Kim, J., Scott, S. V., Oda, M. N., and Klionsky, D. J. (1997). Transport of a large oligomeric protein by the cytoplasm to vacuole protein targeting pathway. J. Cell Biol. *137*, 609–618.

Kirisako, T., Baba, M., Ishihara, N., Miyazawa, K., Ohsumi, M., Yoshimori, T., Noda, T., and Ohsumi, Y. (1999). Formation process of autophagosome is traced with Apg8/Aut7p in yeast. J. Cell Biol. *147*, 435–446.

Legakis, J. E., Yen, W.-L., and Klionsky, D. J. (2007). A cycling protein complex required for selective autophagy. Autophagy *3*, 422–432.

Levine, B., and Klionsky, D. J. (2004). Development by self-digestion: molecular mechanisms and biological functions of autophagy. Dev. Cell *6*, 463–477.

Longtine, M. S., McKenzie, A., III, Demarini, D. J., Shah, N. G., Wach, A., Brachat, A., Philippsen, P., and Pringle, J. R. (1998). Additional modules for versatile and economical PCR-based gene deletion and modification in *Saccharomyces cerevisiae.* Yeast *14*, 953–961.

Mukaiyama, H., Oku, M., Baba, M., Samizo, T., Hammond, A. T., Glick, B. S., Kato, N., and Sakai, Y. (2002). Paz2 and 13 other *PAZ* gene products regulate vacuolar engulfment of peroxisomes during micropexophagy. Genes Cells *7*, 75–90.

Nakatogawa, H., Ichimura, Y., and Ohsumi, Y. (2007). Atg8, a ubiquitin-like protein required for autophagosome formation, mediates membrane tethering and hemifusion. Cell *130*, 165–178.

Noda, T., Kim, J., Huang, W.-P., Baba, M., Tokunaga, C., Ohsumi, Y., and Klionsky, D. J. (2000). Apg9p/Cvt7p is an integral membrane protein required for transport vesicle formation in the Cvt and autophagy pathways. J. Cell Biol. *148*, 465–480.

Noda, T., Matsuura, A., Wada, Y., and Ohsumi, Y. (1995). Novel system for monitoring autophagy in the yeast *Saccharomyces cerevisiae.* Biochem. Biophys. Res. Commun. *210*, 126–132.

Puig, O., Caspary, F., Rigaut, G., Rutz, B., Bouveret, E., Bragado-Nilsson, E., Wilm, M., and Seraphin, B. (2001). The tandem affinity purification (TAP) method: a general procedure of protein complex purification. Methods *24*, 218–229.

Reggiori, F., Black, M. W., and Pelham, H.R.B. (2000). Polar transmembrane domains target proteins to the interior of the yeast vacuole. Mol. Biol. Cell *11*, 3737–3749.

Reggiori, F., Shintani, T., Nair, U., and Klionsky, D. J. (2005). Atg9 cycles between mitochondria and the pre-autophagosomal structure in yeasts. Autophagy *1*, 101–109.

Reggiori, F., Tucker, K. A., Stromhaug, P. E., and Klionsky, D. J. (2004a). The Atg1-Atg13 complex regulates Atg9 and Atg23 retrieval transport from the pre-autophagosomal structure. Dev. Cell *6*, 79–90.

Reggiori, F., Wang, C.-W., Nair, U., Shintani, T., Abeliovich, H., and Klionsky, D. J. (2004b). Early stages of the secretory pathway, but not endosomes, are required for Cvt vesicle and autophagosome assembly in *Saccharomyces cerevisiae.* Mol. Biol. Cell *15*, 2189–2204.

Robinson, J. S., Klionsky, D. J., Banta, L. M., and Emr, S. D. (1988). Protein sorting in *Saccharomyces cerevisiae*: isolation of mutants defective in the delivery and processing of multiple vacuolar hydrolases. Mol. Cell. Biol. *8*, 4936–4948.

Shintani, T., and Klionsky, D. J. (2004a). Autophagy in health and disease: a double-edged sword. Science *306*, 990–995.

Shintani, T., and Klionsky, D. J. (2004b). Cargo proteins facilitate the formation of transport vesicles in the cytoplasm to vacuole targeting pathway. J. Biol. Chem. *279*, 29889–29894.

Stromhaug, P. E., Reggiori, F., Guan, J., Wang, C.-W., and Klionsky, D. J. (2004). Atg21 is a phosphoinositide binding protein required for efficient lipidation and localization of Atg8 during uptake of aminopeptidase I by selective autophagy. Mol. Biol. Cell *15*, 3553–3566.

Suzuki, K., Kirisako, T., Kamada, Y., Mizushima, N., Noda, T., and Ohsumi, Y. (2001). The pre-autophagosomal structure organized by concerted functions of *APG* genes is essential for autophagosome formation. EMBO J. *20*, 5971–5981.

Suzuki, K., Kubota, Y., Sekito, T., and Ohsumi, Y. (2007). Hierarchy of Atg proteins in pre-autophagosomal structure organization. Genes Cells *12*, 209–218.

Takeshige, K., Baba, M., Tsuboi, S., Noda, T., and Ohsumi, Y. (1992). Autophagy in yeast demonstrated with proteinase-deficient mutants and conditions for its induction. J. Cell Biol. *119*, 301–311.

Tomashek, J. J., Sonnenburg, J. L., Artimovich, J. M., and Klionsky, D. J. (1996). Resolution of subunit interactions and cytoplasmic subcomplexes of the yeast vacuolar proton-translocating ATPase. J. Biol. Chem. *271*, 10397–10404.

Wang, C.-W., Kim, J., Huang, W.-P., Abeliovich, H., Stromhaug, P. E., Dunn, W. A., Jr., and Klionsky, D. J. (2001). Apg2 is a novel protein required for the cytoplasm to vacuole targeting, autophagy, and pexophagy pathways. J. Biol. Chem. *276*, 30442–30451.

Xie, Z., and Klionsky, D. J. (2007). Autophagosome formation: core machinery and adaptations. Nat. Cell Biol. *9*, 1102–1109.

Xie, Z., Nair, U., and Klionsky, D. J. (2008). Atg8 controls phagophore expansion during autophagosome formation. Mol. Biol. Cell *19*, 3290–3298.

Yen, W.-L., Legakis, J. E., Nair, U., and Klionsky, D. J. (2007). Atg27 is required for autophagy-dependent cycling of Atg9. Mol. Biol. Cell *18*, 581–593.

Yorimitsu, T., Nair, U., Yang, Z., and Klionsky, D. J. (2006). Endoplasmic reticulum stress triggers autophagy. J. Biol. Chem. *281*, 30299–30304.

Young, A.R.J., Chan, E.Y.W., Hu, X. W., Köchl, R., Crawshaw, S. G., High, S., Hailey, D. W., Lippincott-Schwartz, J., and Tooze, S. A. (2006). Starvation and ULK1-dependent cycling of mammalian Atg9 between the TGN and endosomes. J. Cell Sci. *119*, 3888–3900.